Depletion-Induced Phase Separation of Aggregated Whey Protein Colloids by an Exocellular Polysaccharide

ARTICLE *in* LANGMUIR · DECEMBER 1999

Impact Factor: 4.46 · DOI: 10.1021/la990202c

3 AUTHORS, INCLUDING:

Remco Tuinier
Technische Universiteit Eindhoven
116 PUBLICATIONS **2,891** CITATIONS

SEE PROFILE

C.G. (Kees) De Kruif
Utrecht University
243 PUBLICATIONS **10,509** CITATIONS

SEE PROFILE

Depletion-Induced Phase Separation of Aggregated Whey Protein Colloids by an Exocellular Polysaccharide

R. Tuinier,[†,‡] J. K. G. Dhont,[§] and C. G. De Kruif*[,†,§]

NIZO food research, P.O. Box 20, 6710 BA Ede, The Netherlands, Laboratory of Physical Chemistry and Colloid Science, Wageningen University, Dreijenplein 6, 6703 HB Wageningen, The Netherlands, and Van't Hoff Laboratory, Debye Research Institute, University of Utrecht, Padualaan 8, 3584 CH Utrecht, The Netherlands

Received February 23, 1999. In Final Form: October 6, 1999

An attractive interaction, commonly referred to as depletion interaction, is induced between aggregated whey protein colloid (AWC) particles when they are mixed with exocellular polysaccharides (EPSs) from a lactic acid bacterium. This interaction originates from a loss of conformational entropy of the EPSs near the surfaces of neighboring AWC particles and leads to a phase separation at high enough EPS and AWC concentrations. The effect of the depletion interaction on the properties of the mixtures of EPS and AWC particles is first studied in the stable, that is, one-phase, region. Small-angle neutron scattering (SANS) and dynamic light scattering (DLS) were used to characterize the strength of attractions. The SANS results can be described quantitatively by a model for depletion interaction. From Ornstein−Zernike plots, we derive the position of the spinodal. The DLS results can be described qualitatively quite well by using a recently derived expression for the wavevector (Q)-dependent diffusion coefficient as a function of the correlation length. Further, the experimental phase boundary is determined and compared with a mean-field theory, which evaluates the free energy of a mixture of colloids and large nonadsorbing polymers. The independently calculated spinodal was found to be consistent with the experimentally determined position of the phase boundary. Spinodal phase separation kinetics is investigated by small-angle light scattering (SALS). At low Q, a scattering peak was detected, which shifted to lower Qs with time, in agreement with other experimental data and theoretical predictions for spinodal decomposition. Both the scaling of the scattered intensity with Q and the scaling of the Q-position of the peak with time agree with theoretical predictions.

Introduction

The properties of exocellular polysaccharides (EPSs), produced by food-grade microorganisms during fermentation of milk and products such as yogurt,[1,2] is an important topic for product development but is also of scientific interest. The EPSs have a significant influence on the rheological properties of fermented milk products,[3] but the underlying mechanisms are not yet understood. Adding EPS to a dairy product makes the final product a biopolymer mixture containing polysaccharides and proteins. Both types of biopolymers affect the structure and texture of food products. Upon mixing two such biopolymers in an aqueous solution, they are either associative or segregative. When the biopolymers are mutually segregative, the mixture is said to be incompatible. Incompatibility is a very common phenomenon in polymer solutions as well as in protein−polysaccharide mixtures.[4] Adding polysaccharides to suspensions of globular proteins induces depletion interactions, which lead to an effective mutual attraction between the proteins. Depletion interaction arises from the fact that a polymer molecule loses conformational entropy when confined between neighboring colloidal particle surfaces. This gives rise to depletion of polymer from the region between neighboring protein particles. In the depleted region, the partial osmotic pressure of the polymer molecules is smaller than in the bulk, which leads to an effective attraction between the colloidal particles.

In the present study, we consider the interaction between EPS and (aggregated) whey protein colloids (AWCs). Both components are of practical and scientific relevance. The EPS used can be described as a random coil polymer with a low polydispersity.[5] The AWC particles are well characterized and controlled in size and are representative of many other practical systems. In our EPS/whey protein mixtures, the polysaccharides in solution are much larger than the proteins. An overview of the existing depletion theories, as given by Jenkins and Snowden,[6] shows that the description of mixtures with relatively small polymer molecules and large spheres is well developed. This is not the case for systems with relatively large polymer molecules and small spheres, as used in the present study.

The AWC-particles consist of aggregates of whey proteins and globular proteins with diameters in the range of 2−6 nm. Whey proteins constitute 20% of the proteins in bovine milk. They consist mainly of β-lactoglobulin (50% of the whey proteins), α-lactalbumin, bovine serum albumin (BSA), and immunoglobulins.[7] Upon heating whey proteins above 60 °C, a common (required) treatment in the dairy and food industry, thiol/disulfide exchange

* Corresponding author. E-mail: dekruif@nizo.nl.
† NIZO food research.
‡ Present affiliation: Wageningen University.
§ University of Utrecht.

(1) Cerning, J. *FEMS Microbiol. Rev*. **1990**, *87*, 113.
(2) Abbad Andaloussi, S.; Talbaoui, H.; Marczak, R.; Banally, R. *Appl. Microbiol. Biotechnol.* **1995**, *43*, 995.
(3) van Marle, M. E. Ph.D. Thesis, Twente University, The Netherlands, 1998.
(4) Grinberg, V. Ya.; Tolstoguzov, V. B. *Food Hydrocolloids* **1997**, *11*, 145.
(5) Tuinier, R.; Zoon, P.; Olieman, C.; Cohen Stuart, M. A.; Fleer, G. J.; de Kruif, C. G. *Biopolymers* **1999**, *49*, 1.
(6) Jenkins, P.; Snowden, M. *Adv. Colloid Interface Sci.* **1996**, *68*, 57.
(7) Fox, P. F. In *Developments in Dairy Chemistry*: *4. Functional Milk Proteins*, Fox, P. F., Ed.; Elsevier: London, 1989.

10.1021/la990202c CCC: $19.00
Published on Web 12/10/1999

reactions lead to the formation of intermolecular disulfide bonds of the whey proteins, which leads to aggregation.[8,9]

It is known that mixing dextran with the whey protein BSA leads to phase separation.[10] Mixing native whey proteins with EPS did not lead to a phase separation. This is explained by the fact that the reduction in the possible number of conformations of the polymer molecules in the neighborhood of the colloids decreases with decreasing colloid radius. The native whey proteins are thus too small to induce phase separation of mixtures with EPS.

We have also mixed the EPS with AWCs with a radius of about 30 nm, and these mixtures do exhibit a phase separation, even though the aggregates are still substantially smaller than the EPS (with a radius of gyration of 86 nm).[5] In this paper, we consider the properties of such EPS/AWC mixtures. We first investigate equilibrium and transport properties in the one-phase region, followed by the determination of the experimental phase diagram. This phase diagram is described by a recent mean-field theory by Schaink and Smit[11] for mixtures of small spheres in the presence of long polymers. Finally, we study phase separation kinetics in the unstable (two phase) region.

Theory

In this theoretical section, we first describe the background of the scattering techniques that enable the characterization of the AWCs and of the attractions between the whey protein aggregates induced by EPS. Next, we briefly summarize a theory which gives a description of the phase boundary for small particles and large polymers. In the last section, we shortly review theoretical descriptions on spinodal decomposition, which will be used to describe the phase separation kinetics.

Static Scattering. *Analysis of Molar Mass and Radius of Gyration.* In a (static) light scattering experiment, one measures the scattered intensity $I(Q)$, which is commonly normalized to give the Rayleigh ratio $R(Q)$. The scattered intensity is a function of the wavevector Q, which equals $4\pi\sin(\theta/2)/\lambda$, where θ is the scattering angle and λ is the wavelength of the light in the medium. For polarized light, the scattered intensity, as measured from a homodisperse colloidal suspension, is proportional to the structure factor $S(Q)$ and the particle scattering form factor $P(Q)$:[12]

$$R(Q) = KcMP(Q)S(Q) \tag{1}$$

where c represents the particle mass concentration, M the molar mass of the particle, and K a material constant which depends on the optical contrast and the wavelength. Equation 1 is also valid for small-angle neutron scattering (SANS), for which K depends on the scattering length density difference between solvent and scattering particle. For dilute particle suspensions, $S(Q) \approx 1$, so that at low Q (where $1/P(Q) \approx 1 + Q^2R_g^2/3$) eq 1 becomes

$$\frac{Kc}{R(Q)} \approx \frac{1}{M}\left(1 + \frac{Q^2R_g^2}{3}\right) \tag{2}$$

which shows that a plot of $Kc/R(Q)$ versus Q^2 yields the radius of gyration R_g and the molar mass. This equation will be used to determine the molar mass and radius of gyration of the AWC particles.

Influence of Interactions on the Scattered Intensity. For concentrated suspensions of colloids, the structure factor $S(Q)$ deviates from unity. The structure of a colloidal suspension, hence $S(Q)$, is strongly affected by the interactions between colloidal particles. Upon adding nonadsorbing polymer molecules to a colloidal suspension, the attractions will therefore affect the scattered intensity. The structure factor is equal to the Fourier transform of the radial distribution function $g(r)$:[13]

$$S(Q) = 1 + \rho\int(g(r) - 1)e^{-i\cdot\mathbf{Q}\cdot\mathbf{r}}\,d\mathbf{r} \tag{3}$$

where r is the distance from the center of any particle chosen at random, and ρ is the average number density of the particles. A boldface symbol is a vector. The radial distribution function describes the probability of finding a particle at a distance r from the center of another particle. It is obvious that $g(r)$ changes when particle interactions are changed. The radial distribution function $g(r)$ equals h(r) + 1, where $h(r)$ is the total correlation function, connected to the direct correlation function $c(r)$ through the Ornstein−Zernike relation[14] as

$$h(r) = c(r) + \rho\int c(r_{13})h(r_{23})\,d\mathbf{r}_3 \tag{4}$$

In eq 4, r_{13} equals $|r_1 - r_3|$, r_{23} equals $|r_2 - r_3|$, and $r = |r_1 - r_2|$. The direct correlation function $c(r)$ can be linked to the pair-interaction potential $U(r)$, for instance, by the hypernetted chain (HNC) closure:[15]

$$c(r) = h(r) - \ln[g(r)] - \frac{U(r)}{k_BT} \tag{5}$$

Equations 4 and 5 can be numerically solved by a procedure developed by Gillian.[16] For depletion interactions, which are dealt with in the present study, one can insert a depletion interaction potential in eq 5, and eqs 4 and 5 can be solved, after which eq 3 allows an evaluation of $S(Q)$.

Dynamic Light Scattering (DLS). By means of DLS, we will determine the effect of EPS on the apparent diffusion coefficient of the AWCs. At high colloid concentrations, where interactions between the AWCs are of importance, the diffusion coefficient becomes wavevector-dependent. The apparent diffusion coefficient $D(Q)$ then depends on hydrodynamic interactions and on the structure factor. Near the spinodal, the structure factor behaves as[14,17]

$$S(Q) \sim \frac{1}{\xi^{-2} + Q^2} \tag{6}$$

where ξ is the correlation length, which increases with increasing attraction and goes to infinity at the spinodal. Equation 6 can be derived from the Ornstein−Zernike relation, eq 4 (assuming that $c(r)$ is always short-ranged). A plot of $[S(Q)]^{-1}$ versus Q^2, which gives the correlation length, is therefore referred to as an Ornstein−Zernike

(8) Hoffmann, M. A. M.; Van Mil, P. J. J. M. *J. Agric. Food Chem.* **1998**, *45*, 2942.
(9) Hoffmann, M. A. M.; Roefs, S. P. F. M.; Verheul, M.; Van Mil, P. J. J. M.; de Kruif, C. G. *J. Dairy Res.* **1996**, *63*, 423.
(10) Smit, J. A. M.; Schaink, H. M. *Ind. Proteins* **1995**, *2*, 8.
(11) Schaink, H. M.; Smit, J. A. M. *J. Chem. Phys.* **1997**, *107*, 1004.
(12) Kerker, M. *Scattering of light and other electromagnetic radiation*; Academic Press: New York, 1969.
(13) McQuarrie, D. A. *Statistical Mechanics*; Harper & Row: New York: 1976.
(14) Ornstein, L. S.; Zernike, F. *Proc. Acad. Sci.* **1914**, *17*, 793.
(15) van Leeuwen, J. M. J.; Groeneveld, J.; de Boer, J. *Physica* **1959**, *25*, 792.
(16) Gillan, M. J. *Mol. Phys.* **1979**, *38*, 1781.
(17) Dhont, J. K. G. *An Introduction to Dynamics of Colloids*; Elsevier Science: Amsterdam, 1996.

plot. The collective diffusion coefficient $D(Q)$ near the spinodal is given by[17]

$$D(Q) = D_0\Big[\Sigma(\xi^{-2} + Q^2) + \frac{3a}{4\xi}(Q\xi)^{-2}[1 + (Q\xi)^2 + ((Q\xi)^3 - (Q\xi)^{-1})\arctan(Q\xi)]\Big] \quad (7)$$

where a is the particle radius, Σ is a system-dependent constant (independent of the particle concentration), and D_0 is the Stokes−Einstein diffusion coefficient. The second term within the square brackets was found by Kawasaki[18] in connection with the diffusion of molecular fluid and is often referred to as the Kawasaki function. Equation 7 gives a Q-dependent description of D as a function of the correlation length. We will use eq 7 to interpret our measured DLS data of the AWC particles in the presence of EPS.

Depletion Interaction Theory. In the preceding sections, we discussed how attractions induce measurable phenomena in the one-phase region. This section deals with the prediction of the phase boundary. Asakura and Oosawa[19] initiated the quantitative description of depletion interaction between parallel plates as induced by nonadsorbing polymers. They pointed out that the attractive force between two colloidal particles is proportional to the osmotic pressure of the polymer solution for comparably small polymers. Vrij[20] developed a quantitative theory for depletion forces between two hard spheres as induced by the presence of nonadsorbing polymer molecules; this model can also describe the phase boundary. The polymer molecules, with a radius of gyration R_g, have an effective depletion diameter σ_p and are assumed to behave as mutually ideal but as "hard spheres" with a diameter σ_p toward the colloids. For $r < \sigma_c$, Vrij takes $U(r) = \infty$ and for $r > [\sigma_c + \sigma_p]$, $U(r) = 0$. In the range $\sigma_c < r < [\sigma_c + \sigma_p]$, Vrij derived for the potential:[20]

$$U(r) = -\frac{1}{6}\pi(\sigma_c + \sigma_p)^3\left[1 - \frac{3r}{2(\sigma_c - \sigma_p)} + \frac{r^3}{2(\sigma_c + \sigma_p)^3}\right]\frac{c_p RT}{M} \quad (8)$$

where the factor $c_p RT/M$ is just the osmotic pressure Π_p of the polymer solution, with polymer concentration c_p. Here, M is the molar mass of the polymer, and R and T have their usual meanings. For $\sigma_c > 2R_g$, the effective diameter σ_p approximately equals two times R_g. If the polymers become larger than the colloids, that is, $2R_g > \sigma_c$ as in our case for AWCs and EPS, the effective depletion layer thickness becomes smaller: $\sigma_p < 2R_g$. Since the thermodynamic theories for depletion interaction of Vrij[20] and Lekkerkerker et al.[21] have been developed for $\sigma_c > \sigma_p$, these descriptions cannot be applied to our system. Therefore, we use the theory of Schaink and Smit,[11] who developed a mean field theory that describes the depletion-induced phase (meta-)stability of a suspension of relatively small spherical colloids and long polymer molecules. We will use this theory as a simple approximation in order to describe the experimental data. We briefly summarize the outline of their theory.

Schaink and Smit use a statistical mechanics approach.[22,23] Their starting point is a perturbation expansion of the free energy of the system, F_{tot}, consisting of the free energy of the hard spheres, F_c, which is approximated by the Carnahan−Starling equation of state.[24] The perturbation is the free energy of the polymer solution F_p. Schaink and Smit expressed the contributions to F_p as a spatial integral of the local free energy density $f_p^{tot}(\mathbf{r})$:

$$F_p = \int f_p^{tot}(\mathbf{r})\, d\mathbf{r} = \int (f_p^{tr}(\mathbf{r}) + f_p^{ex}(\mathbf{r}) + f_p^{sg}(\mathbf{r}))\, d\mathbf{r} \quad (9)$$

where $f_p^{tr}(\mathbf{r})$ is the translational entropy of the chains,[25−27] $f_p^{ex}(\mathbf{r})$ accounts for the excluded volume interactions between disconnected polymer segments,[27] and $f_p^{sg}(\mathbf{r})$ is the square gradient contribution which accounts for the restrictions on the possible chain conformations in the neighborhood of the spheres.[25,26] The integration in eq 9 has to be performed over the volume not occupied by the spheres. The determination of the polymer segment concentration profiles is calculated using a cell model in order to simplify the system. The central assumption in the cell model is that the depletion profiles of the polymer segments follow the surface of the nearest sphere. In a first approximation, it is possible to treat the system as a set of N_C cells, where N_C represents the number of AWC particles. In this approximation, the cells are assumed to have a spherical geometry with a volume $4\pi R_L^3/3$, where R_L is the radius of the spherical cell. All length scales are normalized with the Kuhn length l_K. The protein particle is centered in the cell. The cell thus consists of a sphere surrounded by a shell. The shell contains the polymer solution and includes the depletion layer. Within a single cell, it is possible to calculate the polymer concentration profile $p^2(r)$, defined as $\varphi_p(\mathbf{r})/\varphi_p$, by minimizing the polymer free energy within the cell. It is assumed that the polymer segment density profiles of all cells are equal. Since the total volume $V = N_c 4\pi R_L^3/3$ and $V = N_c \pi\sigma_c^3/6\phi$, R_L equals $\sigma_c\phi^{-1/3}/2$. The protein particles are now treated as being isolated, which certainly is an approximation. Using geometrical arguments, the spherical cells are corrected for sphere-cell and cell−cell correlations using hypothetical concentration layers in the cell. Using this model, the total free energy can be calculated as a function of the colloid and polymer concentrations and yields the spinodal, which is a reasonable approximation of the experimental phase line of biopolymer mixtures.[28]

Phase Separation Kinetics. Strong attractions between colloids may induce phenomena like spinodal decomposition or fractal aggregation. Although seemingly quite different, these processes are difficult to distinguish by scattering experiments. Recently, it has been shown that for both diffusion-limited cluster aggregation (DLCA) and spinodal decomposition (SD) the evolution of the structure factor in time is very comparable; there are various close similarities between fractal aggregation and spinodal decomposition.[29,30] The processes can be characterized by determining the fractal dimension d_f of the

(18) Kawasaki, K. *Ann. Phys.* **1970**, *61*, 1.
(19) Asakura, S.; Oosawa, F. *J. Chem. Phys.* **1954**, *22*, 1255.
(20) Vrij, A. *Pure Appl. Chem.* **1976**, *48*, 471.
(21) Lekkerkerker, H. N. W.; Poon, W. C. K.; Pusey, P. N.; Stroobants, A.; Warren, P. B. *Europhys. Lett.* **1992**, *20*, 559.
(22) Lekkerkerker, H. N. W. *Colloids Surf.* **1990**, *51*, 419.
(23) Meijer, E. J.; Frenkel, D. *Phys. Rev. Lett.* **1991**, *67*, 1110.
(24) Carnahan, N. F.; Starling, K. E. *J. Chem. Phys.* **1970**, *53*, 600.
(25) Grosberg, A. Y.; Khoklov, A. R. *Statistical Physics of Macromolecules*; AIP: New York, 1994.
(26) De Gennes, P. G. *Scaling Concepts in Polymer Physics*; Cornell University Press: Ithaca, 1979.
(27) Flory, P. J. *Principles of Polymer Chemistry*; Cornell University Press: New York, 1953.
(28) Tuinier, R.; de Kruif, C. G. *J. Chem. Phys.* **1999**, *110*, 9296.
(29) Ramírez-Santiago, G.; González, A. E. *Physica A* **1997**, *236*, 75.
(30) Poon, W. C. K.; Haw, M. D. *Adv. Colloid Interface Sci.* **1997**, *73*, 71.

aggregating clusters. The evolution of the scattered intensity during a spinodal decomposition obeys a scaling $I(Q) \sim Q^{-3}$ at high Q in the early stages.[29,31] For DLCA, $d_f = 1.75-1.80$, as found from 3D computer simulations of Jullien et al.;[32] this agrees, for instance, with the experimental finding of Weitz and Oliveria,[33] who found $d_f = 1.75$ for fractal aggregating gold sols. For fractal systems we have[34]

$$I(Q) \sim Q^{-d_f} \tag{10}$$

for $a_{low} < 2\pi/Q < a_{up}$, where a_{low} and a_{up} refer to the upper and lower length scale limits in the system, respectively. Upon measuring the scattered intensity as a function of Q for demixing systems with AWC particles and EPS, we found $d_f = 3$. Therefore, our small-angle light scattering results will be compared with theory for spinodal decomposition.

Since the development of the theory for spinodal decomposition by Cahn and Hilliard,[35] it turned out that a wide range of systems could be described with this mechanism. A theoretical discussion of the spinodal decomposition of colloids in the initial and intermediate stages can be found in ref 17. After a quench into the two-phase region, spontaneous fluctuations in density are no longer stable with respect to a homogeneous distribution. The diffusion coefficient in a Fickian type of law then becomes negative, so that certain density fluctuations tend to grow in time. The evolution of density fluctuations can be divided into four stages: an initial, an intermediate, a transition, and a final stage.[17,36] Siggia[37] only distinguishes two stages: an early (initial + intermediate) and a late (transition and final) stage. The theory of Cahn and Hilliard only applies to the initial and intermediate stages, where the density waves have a small gradient. In the initial stage, in addition, the amplitude of density waves is small.

The Cahn-Hilliard theory predicts that during the early stage of the SD process there is a fastest-growing density variation with a typical length scale $\Lambda = 2\pi/Q_m$, with Q_m the wavevector where the scattered intensity has its maximum. In the initial stage, the peak of the scattered intensity $I(Q)$ lies at a fixed Q_m value. The value of Q_m is affected by hydrodynamic interactions only in the intermediate stage (and later stages). Beyond the initial stage, normalization of the $I(Q)$ curves can be used to investigate whether the data can be described as a universal mastercurve by plotting $I(Q)/I(Q_m)$ as a function of Q/Q_m. For spinodal decomposition in the final stage (off-critical conditions), Furakawa[36] proposed the following scaling relation:

$$\frac{I(Q)}{I(Q_m)} = \frac{3(Q/Q_m)^2}{2 + (Q/Q_m)^6} \tag{11}$$

which we will compare with our results. In the final stage, the temporal evolution of density inhomogenities can proceed through coalescence of droplets, as described by Lifshitz and Slyzov.[38] Large clusters with size Λ coalesce with other clusters in a diffusion time $\tau \sim \Lambda^2/D$. By using the Stokes−Einstein equation $D = k_B T/(6\pi\eta_s\Lambda)$ the following differential equation for growth of the droplets can be derived:

$$\frac{d\Lambda^3(t)}{dt} \sim \frac{k_B T}{\eta_s} \tag{12}$$

where η_s is the solvent (medium) viscosity. From eq 12, it follows that $Q_m \sim t^{-1/3}$. Siggia[37] later showed that for concentrated mixtures, the coarsening kinetics is governed by hydrodynamics and the scaling changes to $Q_m \sim t^{-1}$. In the final stage, Q_m reaches a minimum value, and the scattering is then dominated by sharp interfaces which leads to a $I(Q) \sim Q^{-4}$ scaling, known as Porod behavior.[39] We will present experimental small-angle light scattering results of mixtures of AWC and EPS and compare the trends found in our experiment with the theoretical results above.

Methods and Materials

Experimental Techniques. *Small-Angle Neutron Scattering (SANS).* The SANS experiments were made at the Institute Max Von Laue-Paul Langevin (ILL) in Grenoble (France) using the D-22 spectrometer. Hellma QS quartz cells were used with a sample path length of 2 mm. For the required Q-range, we chose sample−detector distances of 14.4 and 18 m. The wavelength of the (cold) emitted neutrons was 1.0 nm with a width of 9%. A circular aperture of 45 mm can be taken to characterize the source size. The scattered intensity of EPS was negligible compared to the scattering of the whey protein aggregates. The EPS molecules themselves thus do not contribute to the scattered intensity of a mixture of AWC aggregates and EPS.

Size Exclusion Chromatography-Static Light Scattering (SEC−SLS). The heated AWC solutions were analyzed by using size exclusion chromatography (SEC). The equipment used consisted of two silica gel columns (Phenomenex TSK) in series, as described by Hoffmann et al.[40] The fractions were analyzed by static light scattering (SLS) with a Wyatt Technology DAWN apparatus equipped with a 5 mW He−Ne laser ($\lambda_0 = 632.8$ nm).

Dynamic Light Scattering (DLS). Dynamic light scattering experiments were performed using a Spectra Physics 275 mW Ar laser with a wavelength of 514.5 nm. The sample cuvette housing was kept at a temperature of 25 °C. The detected photons were processed by a digital ALV-5000 correlator to give the autocorrelation function from which the diffusion coefficient was calculated. We analyzed the data using a second-order cumulant fit.

Small-Angle Light Scattering (SALS). Small-angle light scattering experiments were performed using a Mastersizer X, Malvern Instruments Ltd, which contains detectors at low scattering angles. The cell was always cleaned intensively before a measurement was made. The scattered intensities given in the results section are the measured ones from the mixtures minus the scattered intensity of AWCs at the same concentration without EPS. At very low scattering angles ($<0.2\,\mu m^{-1}$), scattering of dust particles was unavoidable. Correction with the $I(Q)$ of the AWC solutions improved the accuracy in the low Q-range.

Material. *Exocellular Polysaccharide.* The EPS was produced on a pilot-plant scale at NIZO.[5] A *Lactococcus lactis* subsp. *cremoris* NIZO B40 was used to inoculate a whey permeate medium. After production, EPS was isolated using a sequence of filtration steps.[5] This isolate was freeze-dried and used as such in this study. In a previous study,[5] we determined various molecular parameters of B40 EPS. SEC-MALLS analysis of the polysaccharide in aqueous 0.10 M $NaNO_3$ solutions yielded a

(31) Carpineti, M.; Giglio, M. *Phys. Rev. Lett.* **1992**, *68*, 3327.
(32) Jullien, R.; Kolb, M.; Botet, R. *J. Phys. Lett.* **1984**, *51*, 211.
(33) Weitz, D. A.; Oliveria, M. *Phys. Rev. Lett.* **1984**, *52*, 1433.
(34) Texeira. *J. Appl. Crystallogr.* **1988**, *21*, 781.
(35) Cahn, J. W.; Hilliard, J. E. *J. Chem. Phys.* **1958**, *28*, 258; *J. Chem. Phys.* **1959**, *31*, 688.
(36) Furukawa, H. *Physica A* **1984**, *123*, 497.
(37) Siggia, E. D. *Phys. Rev. A* **1979**, *20*, 595.
(38) Lifshitz, I.; Slyzov, V. V. *J. Phys. Chem. Solids* **1961**, *19*, 35.
(39) Porod, G. In: *Small-Angle X-ray Scattering*; Glatter, O., Kratky, O., Eds.; Academic Press: London, 1982.
(40) Hoffmann, M. A. M.; Sala, G.; Olieman, C.; de Kruif, C. G. *J. Agric. Food Chem.* **1997**, *45*, 2949.

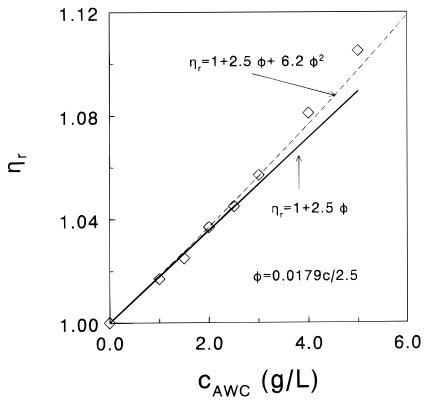

Figure 1. Relative viscosity as a function of AWC concentration, c_{AWC}. Data points represent measurements, and curves represent predictions for hard sphere suspensions.

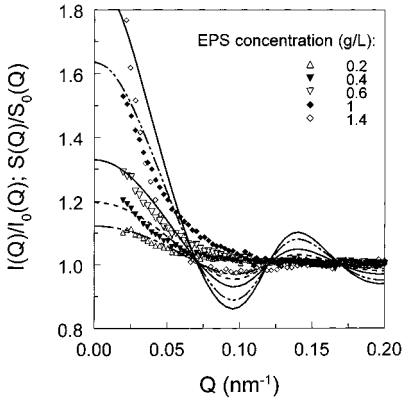

Figure 2. Relative scattered intensity $I(Q)/I_0(Q)$ as measured by SANS for 30 g/L AWC. Results are given for EPS concentrations of 0.2, 0.4, 0.6, 1.0, and 1.4 g/L. The curves are model predictions for the relative structure factor $S(Q)/S_0(Q)$, as obtained from integral theories for polymer concentrations corresponding to the experiments.

number-averaged molar mass of $(1.47 \pm 0.06) \times 10^3$ kg/mol. The radius of gyration (number-averaged) was found to be 86 ± 2 nm. The overlap concentration c^* is thus 0.92 g/L.

Aggregated Whey Protein Colloids (AWCs). Whey protein isolate, produced by Davisco International Inc., USA, was purchased from Domo Food Ingredients, Beilen, The Netherlands. The isolate consisted of β-lactoglobulin (71%), α-lactalbumin (12%), bovine serum albumin (5%), and immunoglobulins (5%). The total amount of proteins in the powder was 93%, and it further contained lactose (0.3%), ash (1.8%), and water (5%). The whey proteins (initial concentration was always 100 g/L) were heated for 2 h at 68.5 °C at pH 7.2 (no salt added). Between 30 and 60 min all native whey proteins were denatured, as determined by a method described earlier.[9,41]

To prevent growth of microorganisms during the experiments, we added 0.02%(w/w) sodium ethylmercurithiosalicylate (C_2H_5-$HgSC_6H_4COONa$−thiomersal, BDH Chemicals) to the mixtures. The protein mixtures containing thiomersal were physically and microbially stable for months.

For the SANS measurements, 99.9% D_2O (Sigma) was used to dissolve the whey proteins and EPS. The pD of the D_2O mixtures was 7.1. Verheul and Roefs[42] investigated the heat-induced aggregation of β-lactoglobulin in D_2O compared to that in H_2O, which showed that the denaturation and aggregation mechanism is hardly affected by D_2O. The main effect is that the overall aggregation process is slowed with D_2O, and we have estimated (personal communication with S. P. F. M. Roefs) that 2.5 h of heating in D_2O should give full denaturation and approximately the same particle size as obtained after heating for 2 h in H_2O.

Characterization of the AWC-Aggregates. From the SEC−SLS analysis of the aggregates, we obtained $R(Q)$ for the various fractions, and from eq 2 we determined R_g and M of each fraction. It was found that the aggregates had a number-averaged radius of gyration R_g of 21 ± 2 nm. Since for a homogeneous sphere the radius of gyration is a factor $\sqrt{(3/5)}$ smaller than the sphere radius, we assumed that the AWC particles have a radius of 27 ± 3 nm. The (number-averaged) molar mass of the aggregates equals $3.6 \pm 0.1 \times 10^3$ kg/mol. By comparing the R_gs and Ms of the various fractions, we obtained $R_g \sim M^{0.33\pm0.01}$, which shows that the "fractal dimension" within an aggregate is 3. The polydispersity expressed as the ratio M_w/M_n, with the weight (M_w) and number-averaged molar mass (M_n), equals 1.28 ± 0.03.

Using DLS, we found the hydrodynamic radius to be 33 ± 3 nm. Within experimental errors, the radii found from SEC−SLS and DLS agree. The radius shall be taken equal to 27 nm in the following discussion. Next, we measured the size of the aggregates in D_2O by DLS. These were prepared by heating for 2.5 h at 68.5 °C in D_2O, and we found a radius of 31 ± 3 nm which, within experimental error, is not different from the aggregates prepared in H_2O.

In Figure 1, we plot the relative viscosity, as measured with an Ubbelohde capillary viscometer, as a function of the whey protein aggregate concentration in the very dilute regime. For very dilute suspensions of colloidal particles, we can use Einstein's expression: $\eta_r = 1 + 2.5\phi$, where η_r is the relative viscosity η/η_s, where η is the solution viscosity and η_s the viscosity of the continuous phase. We find for our data: $\eta_r = 1 + 0.0179c_{AWC}$ and thus $\phi = 0.0179c_{AWC}/2.5$. The specific volume of the AWCs is therefore 7.2 ± 0.5 mL/g. From the radius of gyration and molar mass, the particle density can be calculated, corresponding to 6.5 ± 2.0 mL/g; this agrees with 7.2 ± 0.5 mL/g. Knowing the specific volume makes it possible to convert the AWC concentration into a volume fraction. We have also inserted a curve that follows $\eta_r = 1 + 2.5\phi + 6.2\phi^2$ as derived by Batchelor,[43] where the quadratic term accounts for two-particle interactions.

AWC/EPS Mixtures. EPS and AWC particles were mixed from stock solutions containing usually 5 g/L EPS and concentrated AWC solution. Sodium nitrate was used as salt, and all mixtures were made such that the ionic strength was always set at 0.10 M.

Results and Discussion

This section is divided in three subsections. First, the measurement of the depletion-induced attractions will be considered, followed by a description of the experimental phase diagram as compared with theory. In the last part, we will present measurements that allow an interpretation of the phase separation process.

Attractions. *Small-Angle Neutron Scattering (SANS).* Using SANS, we determined the scattered intensities of AWC solutions at three whey protein concentrations: 25, 30, and 40 g/L, respectively. At each AWC concentration, we prepared a series of samples with varying EPS concentration. Indicative experimental results for 30 g/L AWC are plotted in Figure 2. The results are given as $I(Q)/I_0(Q)$ as a function of Q. The quantity $I_0(Q)$ refers to the scattered intensity of the whey protein aggregates (without EPS), and $I(Q)$ is the scattered intensity of the mixture of AWCs and EPS. The quantity $I(Q)/I_0(Q)$ has the property that any deviation from unity reflects the change of interactions between the proteins induced by the added EPS. Since ϕ and $P(Q)$ are constants for all measurements, and $I(Q) \sim \phi P(Q)S(Q)$, $I(Q)/I_0(Q)$ equals $S(Q)/S_0(Q)$ (where $S_0(Q)$ is the structure factor of AWC without EPS). The assumption $I(Q) \sim \phi P(Q)S(Q)$ is valid for monodisperse systems in the absence of smearing effects. Concerning polydispersity, we assume that for our system we can still use this relation for very low Q, where

(41) De Wit, J. N. *J. Dairy Sci.* **1990**, *73*, 3602.
(42) Verheul, M.; Roefs, S. P. F. M. *FEBS Lett.* **1998**, *421*, 273.
(43) Batchelor. *J. Fluid Mech.* **1972**, *52*, 245.

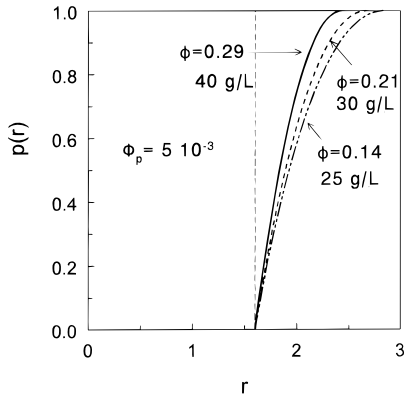

Figure 3. Relative segment concentration $p^2(r)$ as a function of the radius of the spherical cell for a sphere of $R = 1.6$, polymer volume fraction as indicated, and AWC concentrations of 25, 30, and 40 g/L. The corresponding hard sphere volume fraction is given in the plot.

polydispersity hardly influences the structure and form factors (see also Appendix 1). The effect of smearing of the scattering angle and wavelength can be neglected for our system and measuring conditions, as is explained in Appendix 2.

From the plots in Figure 2, we observe an increase of $I(Q)/I_0(Q)$ at small Qs with increasing EPS concentration, which indicates an increase of the structure factor with increasing polymer concentration. We calculated $S(Q)/S_0(Q)$ from integral theory using the HNC closure (eqs 3−5). To do this, we need to estimate the pair-interaction potential $U(r)$. Let us first evaluate the polymer segment density profile in the spherical cell model of Schaink and Smit.[11] We regard the EPS as a flexible polymer with $N_K \approx 150$ Kuhn segments and a Kuhn segment length l_K of 17 nm.[5] In the theory of Schaink and Smit, the sphere radius is normalized with the Kuhn length. This means that the whey proteins, with a radius of 27 nm, have a radius R of 1.6. We calculated the depletion interaction profile in the spherical cell for $\chi = 0.50$, which gave (as will be shown later) the best results for the spinodal for three volume fractions of AWCs. The computed profiles are plotted in Figure 3, where $p(r)$ is the segment concentration of polymer at a distance r relative to that at the radius of the spherical cells, R_L. There is a strong effect of the volume fraction on the segment density profile near the particle surface: a higher volume fraction decreases the depletion layer thickness. From the theory of Schaink and Smit,[11] it follows that the radius of the spherical cell R_L decreases with $\phi^{-1/3}$. According to the mean-field theory of De Gennes,[26] the effective depletion layer thickness δ corresponds to the value of r where $p(r) = \tanh(1) \approx 0.7616$. This expression allowed us to calculate the depletion layer thickness δ ($\equiv \sigma_p/2$) from the polymer concentration profiles $p(r)$. For an AWC concentration of 30 g/L ($\phi = 0.215$), the calculated depletion layer thickness in terms of δ/l_K is 0.51, corresponding to an effective layer thickness of 8.6 nm. This is much smaller than the radius of gyration (86 nm), which is usually taken as the depletion layer thickness for large spheres and small colloids.

To describe the curves in Figure 2, we need an expression for the interaction potential $U(r)$ and subsequently to solve eqs 3−5. We assume the colloids interact via a hard sphere interaction at contact (steep repulsion). For $r > \sigma_c$, we cannot use the expression of Vrij (eq 8), since $2R_g > \sigma_c$. In a simple approximation, we assume that $U(r)/k_BT$ is still proportional to c_p and that the shape is still the same. Due to the complexity of the mixture, we do not know the

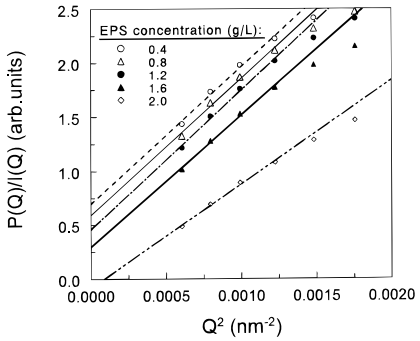

Figure 4. Ornstein−Zernike plots from SANS measurements for 25 g/L AWC at varying EPS concentrations. The curves are best fits to eq 6 in the range $Q^2 < 0.0015$ nm^{-2}.

magnitude. Therefore, we propose

$$\frac{U(r)}{k_BT} = -C_1\left[1 - \frac{3r}{2(\sigma_c + 2\delta)} + \frac{r^3}{2(\sigma_c + 2\delta)^3}\right]c_p \qquad (13)$$

where C_1 is an unknown proportionality constant and the range of the attraction is now given by the depletion layer thickness evaluated from the Schaink−Smit theory. For 30 g/L AWC, we thus use $\delta = 8.6$ nm. By using $U(r)/k_BT = \infty$ for $r < \sigma_c$, $U(r)/k_BT = 0$ for $r > (\sigma_c + \delta)$ (hard sphere approach), and eq 13 for $\sigma_c < r < (\sigma_c + \delta)$, evaluation of eqs 3−5 yields $S(Q)$. We have determined C_1 as follows. First, for each volume fraction of proteins we can calculate c_p at the spinodal from the theory of Schaink and Smit.[11] Second, we can calculate for which value of $U(r)/k_BT$ the structure factor at zero wavevector $S(Q = 0)$ diverges at the spinodal. Then we have both $U(r)/k_BT$ and c_p at the spinodal, from which C_1 can be calculated using eq 13. We found a value of C_1 of 0.011 L/g, whereas the Vrij theory would give a value of 0.47 L/g for our system.

The $S(Q)/S_0(Q)$ values obtained in this way are plotted in Figure 2 for corresponding EPS concentrations, and it is shown that theory and experiment give the same quantitative description of the trends at low Q. The increase of $S(Q)/S_0(Q)$ at low Qs is due to effective attractions, and the deviation from unity increases with increasing polymer concentration. It follows that upon increasing the EPS concentration, the whey protein aggregates become effectively more attractive, as described by the applied depletion interaction model. At $Q > 0.07$ nm^{-1}, the theoretical curves exhibit oscillations while the experimental results do not. This can be explained by a strong damping of both $I(Q)$ and $I_0(Q)$ due to polydispersity in both the particle size and the neutron wavelength. The effect of size polydispersity is illustrated in Appendix 1.

In Figure 4, we plot the inverse of the measured scattered intensities times the form factor $P(Q)$ as a function of Q^2 in the low Q-range (Ornstein−Zernike plot) for various EPS concentrations and (as a representative) AWC concentrations of 25 g/L. According to eq 1, $S(Q)^{-1}$ is proportional to the inverse of the scattered intensity $R(Q)(\sim I(Q))$ multiplied by $P(Q)$, which was taken as $P(Q) = \exp(-Q^2R_g^2/3)$, using $R_g = 21$ nm. It is clear from Figure 4 that $P(Q)/I(Q)$ $(\sim S(Q)^{-1})$ depends approximately linearly on Q^2 for $Q^2 < 0.0015$ nm^{-2}. According to eq 6 in the form $S(Q)^{-1} = A(\xi^{-2} + Q^2)$, the ratio of the intercept and the slope gives ξ^{-2}, hence the correlation length ξ. In this way, we calculated ξ values for $c_{AWC} = 25$, 30, and 40 g/L as a function of the EPS concentration, and the results, given as ξ^{-1} as a function of c_p, are plotted in Figure 5. Extrapolation to $\xi^{-1} = 0$ yields the spinodal, which was

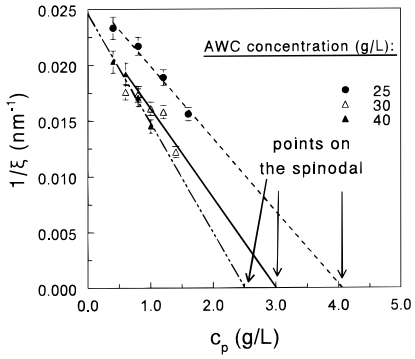

Figure 5. Inverse of the correlation length ξ determined from Ornstein−Zernike plots as a function of the EPS concentration for three AWC concentrations. Drawn curves are linear fits to the data points.

determined from the fit in Figure 5 as 3.9 ± 0.6, 3.0 ± 0.7, and 2.5 ± 0.5 g/L EPS, respectively.

Dynamic Light Scattering. We measured the diffusion coefficients of the AWC particles as a function of Q in the range $8 < Q < 30\ \mu m^{-1}$ at various EPS concentrations. Results are presented for 7.5 and 15 g/L AWC in Figure 6a and b, respectively. Upon increasing the EPS concentration, the diffusion coefficient decreases, especially at low Q. A slowing down of collective diffusion is clearly observed. On the spinodal, there is no driving force to oppose very small concentration gradients, and the collective diffusion coefficient goes to zero at $Q = 0$.

Using eq 7, we calculated the effect of increasing the correlation length on $D(Q)$, and we have plotted theoretical curves from the model calculations with fit-parameters Σ and ξ in Figure 6a and b. The values from the fits for the correlation lengths are given in the plots. The value of Σ was always between 0.5 and 1.5. The curves in Figure 6a were plotted with Σ-values of 0.8, 1.4, 1.4, and 1.2, corresponding to 0, 0.25, 0.5, and 1 g/L EPS, respectively. The results for 1.5 and 2.0 g/L EPS (above c^*) are affected due to a significant contribution of EPS to the scattering of the mixture. We therefore did not fit these data to the theoretical prediction of eq 7. The results show that adding EPS increases the correlation length of the AWC particles due to depletion-induced attractions, as also follows from the SANS results. The qualitative correspondence as presented in Figure 6a and b is satisfactory, which shows that both equilibrium properties, such as $S(Q)$, as well as transport properties are affected by changing the EPS concentration in suspensions of globular proteins. Above 15 g/L AWC, the system became too turbid for a reliable measurement of the diffusion coefficient of AWC particles due to multiple scattering.

Phase Diagram. The experimental data given in the preceding section concern mixtures in the one-phase region. Upon increasing either the EPS or the AWC concentration, phase separation will occur when the phase boundary is crossed. The observed phase diagram is presented in Figure 7. The full line is drawn to guide the eye. The open circles indicate stable mixtures. In the unstable region, various types of coexisting phases can be observed, as indicated in Figure 7. First, just above the phase boundary we recognized a two-phase system (filled circles) consisting of an upper phase concentrated in EPS and a lower phase concentrated in AWCs, the latter being viscous when the initial concentration was 30 g/L or higher. The interface was always very sharp. Second, sometimes a third phase was formed (triangles) between the two phases mentioned above. This phase was rather turbid and seemed to arise from whey proteins which sediment

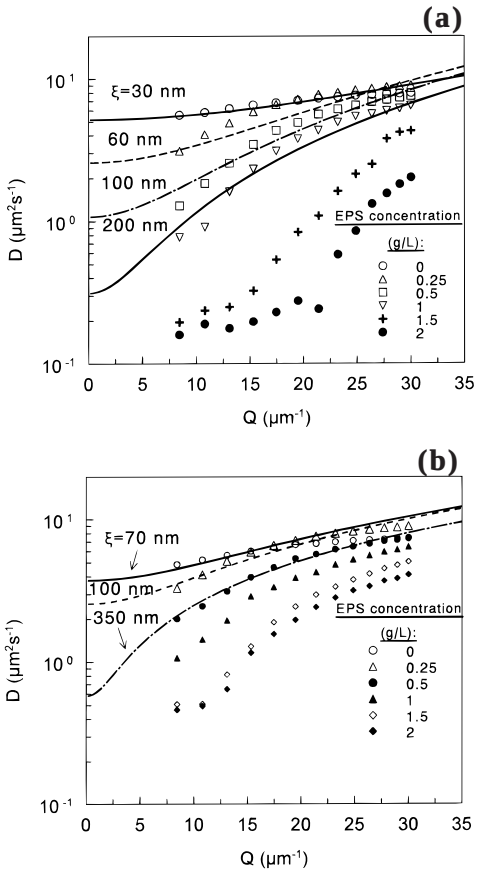

Figure 6. Diffusion coefficients for (a) 7.5 g/L AWC and (b) 15 g/L AWC as a function of Q. The various EPS concentrations are indicated in the plots. The curves were calculated from eq 7, and the correlation lengths, which give a good description of the data, are indicated in the figure.

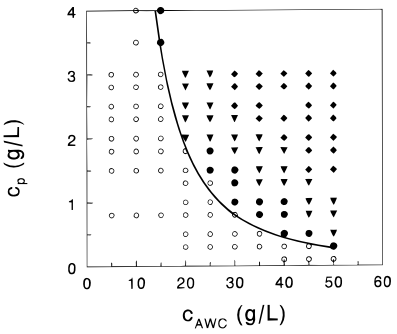

Figure 7. Phase diagram as obtained from visual observation. Polymer concentration is given as a function of the AWC concentration. The drawn line is only a guide to the eye. Open circles refer to stable mixtures. Closed circles are two-phase systems, triangles are two-phase systems with a third turbid middle "phase", and diamonds refer to three-phase systems where one "phase" is a gel.

from the upper phase. Possibly, size fractionation of AWC occurs. Third, we found systems containing three phases from which the lower phase, containing most of the AWCs, is gel-like (diamonds). This is not surprising since aggregating whey proteins are initially somewhat mutually attractive, which enhances gelation (for very short-ranged attractions).

We calculated the total free energy of the mixture F_{tot} from the Schaink−Smit theory[11] and the spinodal. As explained before, we used $\sigma_c = 3.2$ (corresponding to 54 nm) and $N_K = 150$ in the calculations. The results matched best if $\chi = 0.5$ was used in the calculations, although the

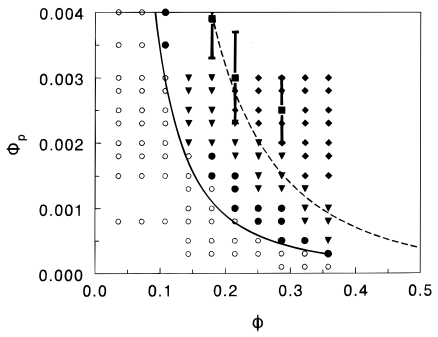

Figure 8. Phase diagram with data points and (full) line to guide the eye, as in Figure 7. The symbols φ_p and ϕ are the volume fractions of polymer and protein aggregates, respectively. The dotted curve is the prediction from the theory of Schaink and Smit,[11] and the gray squares with error bars are the spinodal as determined from SANS; see Figure 5.

χ-dependence of the spinodal is weak. For lower χ-values (or better solvent quality), the spinodal curve shifts to higher polymer concentrations. The theoretical curve for $\chi = 0.5$ is plotted in Figure 8 in terms of the polymer volume fraction φ_p and the AWC volume fraction ϕ. In Figure 8, we have replotted the experimental data, as well as the experimental phase line from the phase diagram given in Figure 7. The whey protein concentrations were converted to ϕ values by using $\phi = 0.0179c_{AWC}/2.5$. The polymer volume fraction φ_p was calculated from c_p/ρ_p, where ρ_p is the bulk density and was taken as 1000 kg/m^3, a common value for polysaccharides.[44] The shapes of the curves as well as the values of the calculated spinodal and the experimental phase boundary (the binodal) correspond satisfactorily.

It should, however, be noted that the theory of Schaink and Smit uses the square gradient approach in order to take into account the presence of an interface. In this approach, one assumes weak gradients and very long polymer chains, and it is therefore assumed that the Kuhn length is short compared to all other length scales.[25] In contradiction, as discussed in the SANS results section, the effective depletion layer thickness is smaller than the Kuhn length for the relevant range of colloid volume fractions. Further, the model of Smit and Schaink[11] was developed for monodisperse polymers and spheres, and our EPS and AWC particles are polydisperse. Therefore, no quantitative agreement can be expected, and in particular no critical point can be determined by combining the experimental binodal and the theoretical spinodal.

In Figure 8, we also added the experimentally determined spinodal points from the SANS measurements (gray squares), using the criterion $\xi^{-1} = 0$ (see Figure 5). These data are in reasonable correspondence with the curve from the theory of Schaink and Smit, which shows that SANS is a good tool to measure attractions and to predict the spinodal from measurements in the one-phase region.

Phase-Separation Kinetics. In the unstable region, the mixtures phase-separate, and the scattered intensity of several of such mixtures was studied by small-angle light scattering (SALS). For several samples (far above the phase line) the transmission was too low to neglect multiple scattering. At very high AWC concentration (>35 g/L), the transmission was also too low to perform accurate measurements for all mixtures. Therefore, our attainable experimental range of AWC concentrations is between the phase boundary and 35 g/L.

In Figure 9a, the time evolution of the scattered intensity as a function of the wavevector is given for a mixture of 30 g/L AWC particles and 1.5 g/L EPS. This system is representative for the evolution of the scattered intensity of the mixtures measured in the unstable region. It is evident that the overall value of the scattered intensity increases in time. All curves go through a maximum in the scattered intensity as a function of Q. The first recorded value of Q_m, the value of Q where $I(Q)$ goes through a maximum, corresponds to a characteristic length scale (the fastest-growing density variation has a typical length scale $\Lambda = 2\pi/Q_m$) Λ of $\sim$9 μm. The large detected sizes agree with the visual observation that unstable mixtures became very turbid. The value of Q_m decreases with time and is independent of time only in the initial stage,[17] which thus occurs on time scales outside our experimental window. Such a time-dependent behavior as we observe is common to spinodally decomposing systems, such as gelatin/dextran mixtures,[45] binary liquid mixtures,[46] adhesive hard sphere suspensions,[47] polymer mixtures,[48] and unstable suspensions of micelles.[49]

In Figure 9b, the scattered intensity is plotted as a function of Q on a log−log scale. As can be seen in Figure 9b, the slope of $\ln\{I(Q)\}$ versus $\ln\{Q\}$ at large Q-values approaches asymptotically -4, as expected for sharp interfaces.[39] We are thus not dealing with aggregation, in which case the slope is equal to the fractal dimension of the aggregates, with an expected slope around -2.[32]

From the maximum of the curves plotted in Figure 9a, we determined the values of Q_m as a function of time and plotted the characteristic length scale Λ ($= 2\pi/Q_m$) in Figure 10 as a function of time. For the mixtures investigated, the exponent generally varied between 0.3 and 0.6. Verhaegh et al.[50] found, for a spinodal decomposition (SD) of unstable mixtures of silica spheres (coated with stearyl alcohol) and PDMS as polymers, an exponent of 1/3 in the earlier stages and a crossover to 1 in the late stage. Their results agree with theoretical predictions of Lifshitz and Slyzov[38] (1/3) for the early stage and Siggia[37] (1) for the late stage. Our results in Figure 10 seem to conform reasonably to these theoretical results.

It is known that rescaling the $I(Q)$ versus Q curves leads to a master curve for systems that exhibit SD. In Figure 11, we plot $I(Q)/I(Q_m)$, where $I(Q_m)$ is the maximum scattered intensity, as a function of Q/Q_m, and we find that within experimental error the data collapse to a single master curve. The dotted curve added in Figure 11 is the prediction of Furukawa[36] for off-critical behavior. The Furukawa prediction differs from the experimental data, especially at high Q. Qualitatively, the same deviation was found by Rouw et al.[47] for an adhesive hard sphere suspension that demixed through SD. The difference might be due to polydispersity, which tends to spread out the scattered intensity over a wider Q-range.

Conclusions

Mixing aggregated whey protein colloids (AWCs) with exocellular polysaccharides leads to a segregative interaction. Small-angle neutron scattering (SANS) and dynamic

(44) Brandrup, J.; Immergut, E. H. *Polymer Handbook*; Wiley: New York, 1989.

(45) Tromp, R. H.; Rennie, A. R.; Jones, R. A. L. *Macromolecules* **1995**, *28*, 4129.

(46) Huang, J. S.; Goldburg, W. I.; Bjerkaas, A. W. *Phys. Rev. Lett.* **1974**, *32*, 921.

(47) Rouw, P.; Woutersen, A. T. J. M.; Ackerson, B. J.; de Kruif, C. G. *Physica A* **1989**, *156*, 876.

(48) Bates, F. S.; Wiltzius, P. *J. Chem. Phys.* **1989**, *91*, 3258.

(49) Wilcoxon, J. P.; Martin, J. E.; Odinek, J. *J. Non-Cryst. Solids* **1994**, *172*, 1142.

(50) Verhaegh, N. A. M.; van Duijneveldt, J. S.; Dhont, J. K. G.; Lekkerkerker, H. N. W. *J. Chem. Phys.* **1996**, *102*, 409.

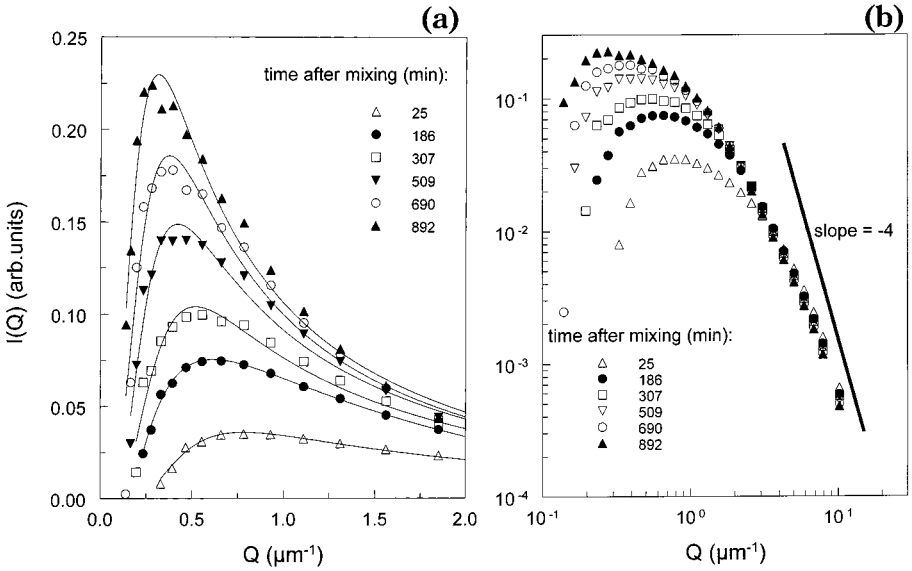

Figure 9. (a) Scattered intensity $I(Q)$ as a function of the wavevector Q measured at various time intervals after mixing EPS and AWC particles. The initial mixture contained 30 g/L AWC and 1.5 g/L EPS. Curves are drawn to guide the eye. (b) Results as in (a) but plotted logarithmically and also for the higher Q-range. The straight line corresponds to Porod behavior: $I(Q) \sim Q^{-4}$.

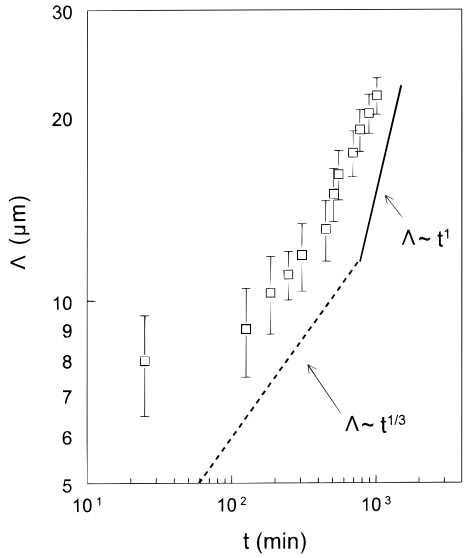

Figure 10. Position of the typical length scale Λ as a function of time after mixing EPS and AWC for the results presented in Figure 9(a). Drawn curves represent the theoretical scaling relations $\Lambda \sim t^{1/3}$ and $\Lambda \sim t$.

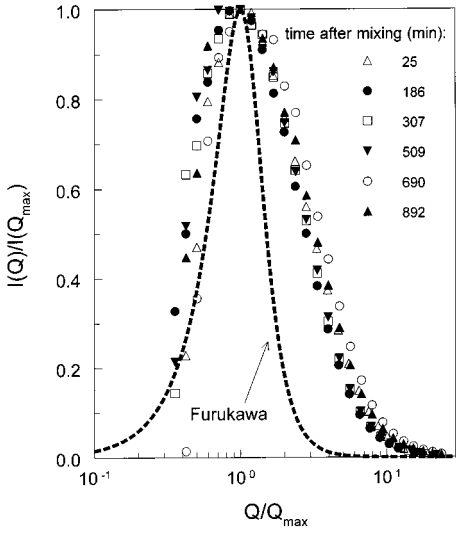

Figure 11. Normalized scattered intensity $I(Q)/I(Q_m)$ as a function of the normalized wavevector Q/Q_m for the results given in Figure 9(a).

light scattering (DLS) experiments can probe effective attractions between the protein colloids. The SANS results could be quantitatively described by a depletion interaction model, and the results from DLS could be described qualitatively. Ornstein−Zernike plots allowed a calculation of the correlation length of the AWC particles. From these correlation lengths, the spinodal was calculated for three whey protein concentrations; this spinodal lies above the binodal as determined by visual observation but is within the same order of magnitude.

The spinodal was also calculated from a recently developed mean-field theory. The calculated spinodal and the shape of the curve of the theoretical prediction are consistent with the observed phase diagram. The spinodal as determined from SANS lies between the experimental binodal and the theoretical prediction for the spinodal.

Small-angle light scattering experiments were performed to detect the temporal evolution of the scattered intensity of mixtures in the unstable region. The results showed that the phase separation could be described as a spinodal decomposition on the basis of scaling arguments.

Acknowledgment. The Netherlands Association of Biotechnology Centers (ABON) financially supported this work. Dominique Ginapé and Alexandra Le Roy are thanked for performing many experiments. Jan van Riel, NIZO food research, is thanked for performing the SEC-MALLS measurements. The help of and discussions with Dr. C. Holt (Hannah Research Institute, UK) and Dr. P. A. Timmins (ILL, Grenoble, France) concerning the SANS experiments are highly appreciated. Dr. H.M. Schaink, University of Twente, Rheology Group, is thanked for useful discussions and for providing us with his computer program which made possible the mean-field calculations. We thank Dr. P. van der Schoot (Van't Hoff laboratory, Utrecht University), Drs. P. J. J. M. van Mil, S. P. F. M. Roefs, E. ten Grotenhuis, and R. H. Tromp (NIZO food research) for useful discussions. Professor G.J. Fleer (Laboratory for Physical Chemistry and Colloid Science,

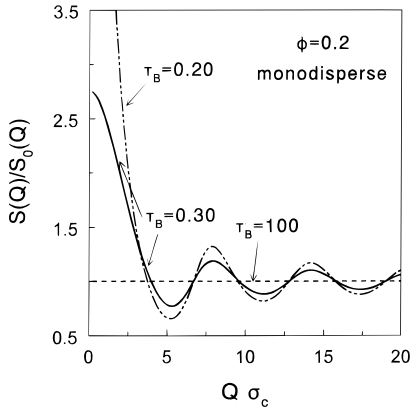

Figure 12. Relative structure factor $S(Q)/S_0(Q)$ as a function of $Q\sigma_c$ for monodisperse adhesive hard spheres with varying stickiness.

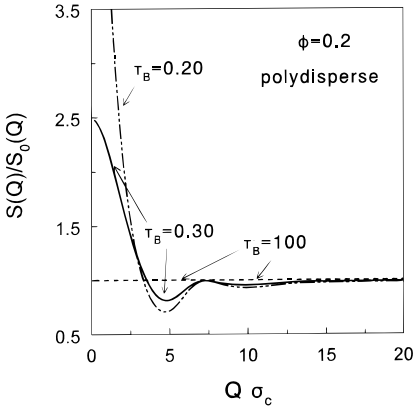

Figure 13. As in Figure 12, for particles with a Schulz−Flory size distribution with a standard deviation of 20%.

Wageningen University) is thanked for a critical reading of the manuscript.

Appendix 1

The calculated curves in Figure 2 give a good description of the experimental data in the low Q range, but for higher values ($Q > 0.07$ nm^{-1}), the theoretical predictions exhibit oscillations around unity whereas the experimental data converge to unity without showing oscillations. This difference is due to polydispersity in size of the AWC particles, the EPSs, and polydispersity in neutron wavelength. It is beyond the scope of this study to extend the theory in order to account for polydispersity in size of the particles. However, use can be made of the model developed by Robertus et al.[51] for the scattering of polydisperse adhesive hard spheres. In Figure 12, we plot the calculated results for $S(Q)/S_0(Q)$ for a suspension of monodisperse colloids with a volume fraction of 0.2. Here, $S(Q)$ is the structure factor of an adhesive hard sphere suspension with a certain adhesiveness, expressed by the Baxter parameter τ_B,[52,53] and $S_0(Q)$ is the structure factor of a hard sphere suspension. The results are given for three values of the Baxter parameter: $\tau_B = 100$, 0.30, and 0.20, corresponding to an increasing effective attraction. The oscillations are clearly visible over the plotted Q-range. In Figure 13, the results are plotted for colloidal particles that have a dispersion in size according to a Schulz-Flory distribution with a standard deviation of 20% for the same volume fraction and adhesiveness as in Figure 12. Although at low Q (below $Q\sigma_c \approx 5$) the results are almost identical, at higher Q the oscillations in the relative structure factor $S(Q)/S_0(Q)$ have dampened strongly, which illustrates that the difference between experiment and theory at high Q is probably due to polydispersity.

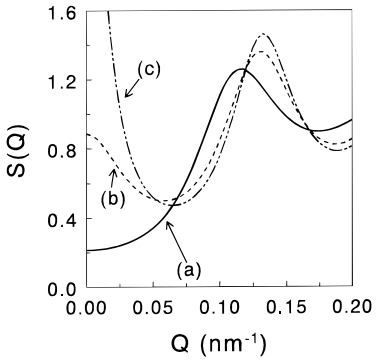

Figure 14. Structure factor $S(Q)$ as a function of Q for hard spheres (HS) with a radius of 27 nm (a) and for spheres with depletion interaction (b and c).

Appendix 2

In this appendix, we investigate the effect of smearing on our data. To estimate the effect of wavelength and scattering angle smearing, we shall use step-functions to describe their distribution. The smeared scattered intensity $I_{sm}(\lambda,\theta)$ can then be written as a function of the scattering intensity in an ideal experiment (no smearing), $I(\lambda,\theta)$, as

$$I_{sm}(\lambda,\theta) = \frac{1}{2\delta\lambda}\int_{\bar{\lambda}-\delta\lambda}^{\bar{\lambda}+\delta\lambda} d\lambda \frac{1}{2\delta\theta}\int_{\bar{\theta}-\delta\theta}^{\bar{\theta}+\delta\theta} d\theta I(\lambda,\theta) \qquad (14)$$

where $\delta\lambda$ and $\delta\theta$ correspond to wavelength and angle smearing, and the dashes above λ and θ refer to their averages. Expansion of $I(\lambda,\theta)$ leads to

$$I_{sm}(\lambda,\theta) \approx I(\bar{\lambda},\bar{\theta}) + \frac{dI(\bar{\lambda})}{d\bar{\lambda}}d\lambda + \frac{dI(\bar{\theta})}{d\bar{\theta}}d\theta + \frac{1}{2}\frac{d^2I(\bar{\lambda})}{d\bar{\lambda}^2}(d\lambda)^2 + \frac{1}{2}\frac{d^2I(\bar{\theta})}{d\bar{\theta}^2}(d\theta)^2 + \frac{d^2I(\bar{\lambda},\bar{\theta})}{d\lambda d\theta}d\lambda d\theta + \ldots \qquad (15)$$

Substitution into eq 14 thus gives, up to term of order $(d\lambda)^2$, $(d\theta)^2$, $(d\lambda d\theta)^2$,

$$I_{sm}(\lambda,\theta) = I(\bar{\lambda},\bar{\theta}) + \frac{1}{6}\left[\frac{d^2I(\bar{\lambda})}{d\bar{\lambda}^2}(d\lambda)^2 + \frac{d^2I(\bar{\theta})}{d\bar{\theta}^2}(d\theta)^2\right] \qquad (16)$$

In terms of Q one can write

$$\frac{d^2I(\lambda)}{d\lambda^2} = \frac{Q}{\bar{\lambda}^2}\left(Q\frac{d^2I(Q)}{dQ^2} + 2\frac{dI(Q)}{dQ}\right) \qquad (17)$$

and

$$\frac{d^2I(\theta)}{d\theta^2} = \frac{Q^2}{\bar{\theta}^2}\frac{d^2I(Q)}{dQ^2} \qquad (18)$$

where we made use of the approximation $Q \approx 2\pi\bar{\theta}/\bar{\lambda}$, which is valid for very low Q. By combining eqs 16−18 we can derive the following expression for the relative difference

(51) Robertus, C.; Philipse, J.; Joosten, J. G. H.; Levine, Y. K. *J. Chem. Phys.* **1989**, *90*, 4482.
(52) Baxter, R. J. *J. Chem. Phys.* **1968**, *49*, 2770.
(53) Penders, M. H. G. M.; Vrij, A. *J. Chem. Phys.* **1990**, *93*, 3704.

between $I_{sm}(\lambda,\theta)$ and $I(\lambda,\theta)$, ν:

$$\nu = \frac{I_{sm}(\lambda,\theta) - I(\lambda,\theta)}{I(\lambda,\theta)} = \frac{1}{6I(\lambda,\theta)}\left[\left(Q^2\frac{d^2I(Q)}{dQ^2} + 2Q\frac{dI(Q)}{dQ}\right)\left(\frac{\delta\lambda}{\bar{\lambda}}\right)^2 + Q^2\frac{d^2I(Q)}{dQ^2}\left(\frac{\delta\theta}{\bar{\theta}}\right)^2\right] \quad (19)$$

To estimate the effect on our result, we calculate ν as a function of Q for the three $S(Q)$ curves plotted in Figure 14. We mimicked our experimental system by taking a volume fraction of 0.215 and a range of attraction of 0.30. Curve (a) corresponds to the structure factor of hard spheres and curves (b) and (c) to hard spheres with a typical depletion interaction. The $S(Q)$s were calculated as described in ref 54. We apply eq 19 to our experimental conditions: a radius of the colloids of 27 nm, a wavelength spread ($\delta\lambda/\bar{\lambda}$) of 9%, a sample−detector distance of 14.4 nm, and a neutron source size with a circular aperture of 45 mm. In Figure 15, we plotted ν as a function of Q for the three theoretical curves plotted in Figure 14. In our results section, we presented curves of $S(Q)/S_0(Q)$. Therefore, we should focus on the absolute value of the sum $\{(a)^2 + (b)^2\}^{1/2}$ or $\{(a)^2 + (c)^2\}^{1/2}$ of the relative deviations. In any case, the deviation is always less than 5% under our conditions. It can therefore be concluded that smearing affects the results but to such a small degree that our experimental data may still be compared directly to theoretical predictions.

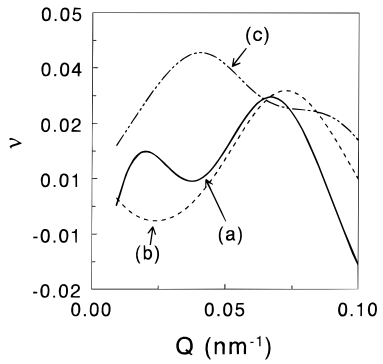

Figure 15. Relative error due to smearing in $S(Q)$ for the systems plotted in Figure 14.

LA990202C

(54) Tuinier, R.; ten Grotenhuis, E.; Holt, C.; Timmins, P. A.; de Kruif, C. G. *Phys. Rev. E* **1999**, *60*, 848.